Advances in Science and Technology Research Journal

Advances in Science and Technology Research Journal, 2026, 20(2), 264–283
https://doi.org/10.12913/22998624/211575
ISSN 2299-8624, License CC-BY 4.0

Received: 2025.09.30
Accepted: 2025.11.15
Published: 2025.12.23

Mechatronic design techniques to predict the best clamping conditions in slender ball end milling of a flexible workpiece

Krzysztof J. Kaliński[1], Natalia Stawicka-Morawska[1*], Marek A. Galewski[1], Michał R. Mazur[1]

[1] Institute of Mechanics and Machine Design, Faculty of Mechanical Engineering and Ship Technology, Gdańsk University of Technology, ul. Narutowicza 11/12, Gdansk, Poland
* Corresponding author's e-mail: natalia.morawska@pg.edu.pl

ABSTRACT

An effective method of minimizing vibrations during milling of small flexible workpieces is presented, using a new modified approach to the problem of vibration reduction, based on a workpiece holder with adjustable clamping stiffness. A completely new formulation of a mechanistic model of cutting dynamics for milling processes was developed. An important novelty is also the discrete modeling of a flexible workpiece in the convention of the rigid finite element method, as well as the inclusion of the rotational speed of a slender cutting tool in the structural model. It is expected to confirm the research hypothesis that the use of dedicated mechatronic design techniques optimizes the effectiveness of the vibration reduction system during milling, taking into account the dynamic conditions of the cutting process and the use of clamping the workpiece on the milling table in a special holder. A three-dimensional mechanistic description of the milling process will improve the behavior and effectiveness of the workpiece vibration reduction system. The research methodology based on selected mechatronic design techniques assumes computer simulation (virtual prototyping – VP) of the tool-workpiece vibration suppression system, experimentally aided virtual prototyping (EAVP) and implementation of vibration suppression in the target system (ITS). An original method of simulation of a computational model of the milling process in hybrid coordinates was developed, the effectiveness of which was confirmed by the results of machining workpieces of bronze CC331G and aluminum alloy EN AW-6101.

Keywords: mechatronic design, clamping condition, stiffness adjustment, modal analysis, ball end milling, flexible workpiece.

INTRODUCTION

Milling operations in general and high-speed milling (HSM) with slender tools of flexible workpieces with spatially complex surfaces and contours are often used in modern machining centers. The technological justification for such operations is rooted in the need for precise generation of complex geometric configurations (e.g. turbine blades, rotors, thin-walled elements, micro-components, etc.). Such components are in great demand to meet the needs of the food, machine building, automotive, aviation, and precision manufacturing industries to mention a few. The complexity of these products and of the associated manufacturing technologies, as well as the high costs of finishing operations, require that the milling process be performed as the "finishing" in the process chain. Because of the global trend of increasing cutting speeds above 1000 m/min and feed rates over 100 m/min, high performance can be achieved with much lower allowances than by conventional operations [1]. The latter is not without significance from the point of view of the reduction of cutting forces [2]. Given the almost total elimination of coolants [3, 4] the processes performed, including high-speed and micro-machining, are becoming ecologically friendly.

The methodology of vibration suppression through spindle speed variation proposed in [5]

was successfully applied in HSM of rigid workpieces by slender tools. The efficiency of this modified method of vibration suppression in the potentially unstable regions of spindle speeds, resulting from the position of stability lobes, was confirmed [6]. Vibration suppression using the method of spindle speed variation, however, is ineffective in the case of milling flexible structures [7]. Instead, the efficiency of the tool-flexible workpiece vibration suppression method was shown during high-speed milling on an Alcera Gambin 120CR and a Mikron VCP600 machine. Spindle speed adjustments also led to the minimization of the work of cutting forces along directions of the corresponding cutting layer thickness [8, 9]. It should be noted that this method has an inability to function over the full spindle speed range [10]. A similar situation is described in [11], where the machine does not fully utilize the available spindle speed range due to limitations of spindle acceleration and deceleration.

Due to their excellent properties, high efficiency and light mass, thin-walled structures are becoming increasingly popular in various industries [12], especially in the aerospace industry [13, 14]. These parts are often produced using materials that are challenging to machine, including titanium alloys [15], and are characterized by low rigidity, limited damping capacity, and substantial material removal requirements during milling operations [16]. Consequently, the thin-wall milling operation is significantly influenced by regenerative chatter vibrations, leading to accelerated tool wear, poor surface integrity, and decreased efficiency [17].

An appropriate milling system model is typically categorized into three categories: rigid tool-flexible workpiece, flexible tool-rigid workpiece, and flexible tool-flexible workpiece [18]. Specifically, thin-wall milling involving slender tools is included in the flexible tool–flexible workpiece category [19]. Formerly, appropriate approaches to chatter suppression were divided into: in-process, out-of-process, active, and passive [17]. However, a more contemporary classification of prediction and suppression methods in thin-wall milling suggests a division of them into passive, active, and semiactive techniques [20].

The need to find optimal conditions for fixing the object in the holder in order to reduce its deformation is of particular importance [21, 22] and the dedicated supporting and fixturing technologies are indicated [23, 24]. The use of different support methods can contribute to minimizing the detrimental effects of vibration and cutting forces [25]. Conventional chatter avoidance methods typically select chatter-free machining parameters using the stability lobe diagram, which necessitates an accurate dynamic model of the thin-wall milling system [26]. However, due to the highly non-linear and time-varying characteristics of the thin-wall cutting process, simplifying assumptions are often necessary, leading to unavoidable prediction errors [27]. Alternatively, the semi-active control method may be considered as an enhanced form of the passive control approach, incorporating the controllable components such as an adjustable spring or damper [28] containing a magnetorheological or electrorheological fluid [29]. The issue of accurate description of the dynamics of the milling process of thin-walled workpieces is also important from the point of view of predicting and reducing chatter vibrations, but it is particularly important when significant machining allowances are applied [30, 31].

The basis of the presented scientific methodology concerns the use and development of dedicated mechatronic design techniques [32]. The prediction of vibration suppression results on the basis of computer simulation of the process machine tool-holder-workpiece-tool (MHWT) calculation model, commonly used in many former scientific and research works, is not always precise. Besides, due to a significant number of degrees-of-freedom, the system/process is so complex that real-time (RT) simulation, needed for on-line control of active systems for workpiece vibration control, is difficult to obtain [33]. On the other hand, utilizing off-line tuned adjustable stiffness holders has demonstrated good efficiency of suppression over a wide range of spindle speeds [34, 35]. The whole system is easier for integration, because of the lack of the necessity for on-line control. A key condition is that the holder stiffness parameters ought to be adjusted in an optimal way. Thus, real-time simulation is not recommended in such a case. Instead of it, the use of experiment-aided virtual prototyping (EAVP) is being proposed here. All the more so as it has been shown that the process of virtual simulation actually fulfils the real-time requirements with respect to time of the actual performance. The latter, together with simulations implemented only on customary computing equipment (i.e. virtual prototyping – VP), are important techniques for mechatronic design, prior to the implementation

of the vibration suppression system on the target plant (ITS), e.g. milling machines operating in continuous motion.

The mechatronic approach to the design process is justified by the fact that several components of the system/process can be designed in parallel, provided that a method exists for checking the compatibility of each element, that is to say: virtual prototyping. Concurrent design offers several advantages, including a shortened design phase, simplifying and accelerating implementation, and greater flexibility in executing individual functions. Properly conducted, with component verification via virtual prototyping, it prevents undesired interactions. Simultaneous development of all components enhances flexible in implementing various device or process functions. While the precise design procedure depends on the device or process, key techniques of mechatronic design include virtual prototyping (VP), experiment-aided virtual prototyping (EAVP), and implementation on the target system (ITS).

DESCRIPTION OF THE PROPOSED METHOD

The research methodology

Virtual prototyping

Virtual prototyping allows for fast and low-cost simulation of many alternatives of the process performance, at the demanded accuracy level. Also, it allows concurrent design, thanks to supported means of verification of the correct interaction between all components. A simulation model is an idealized mathematical description of a real process formulated for a specific class of phenomena. Thus, there is a need for creating a number of models for simulation of various phenomena at various levels of particularity. In addition, full system simulations are too time-consuming so that usually only a few models are created, e.g., one for individual module and one for the whole system. The simulations often disclose that accurately representing workpiece behavior demands highly complex models. Thus, simplified models with parameters adjusted to the desired precision are applied. Models of individual components of the system can be created based on the laws of physics (structural models). The proposed virtual prototyping scheme is shown in Figure 1.

Deliverables of the technique are:

- valuable database for dedicated milling processes;
- simulation programs for suppression of vibrations during milling of flexible structures;
- initial validation of the correctness of determining the optimality condition for vibration suppression of a flexible structure.

Experiment-aided virtual prototyping

The proposed approach consists of (Figure 1):

- using the mechanistic cutting process dynamic characteristics;
- engaging real components of the research system;
- performing off-line experimental identification of the holder-workpiece system's modal parameters,
- computing on-line the tool-workpiece vibrations of the milling process model;
- determining off-line the optimal holder support stiffness;
- evaluating the efficiency of vibration suppression.

Deliverables of the technique are:

- development of the modified method of vibration suppression with the use of the workpiece holder with adjustable support stiffness;
- integration of the computer measurement system, the workpiece, piezoelectric accelerometers and the variable support stiffness holder of the workpiece;
- implementation of the appropriate hardware and own software for the computer simulation and validation of the model parameters.

The efficiency of the portable research stand will be verified, which in the next task will be adapted for milling machines operating in continuous motion. To this end, the specified test apparatus will be supplemented by the specially designed adjustable stiffness holder for flexible workpieces, having the ability of tuning the optimal support stiffness. In addition to the required static stiffness, this holder should ensure dynamic accuracy of the milling process by minimizing the tool-workpiece vibration levels at the instantaneous contact point.

Implementation in the target system

During the implementation of the vibration suppression in the target system, all system components are real. In contrast to experiment-aided simulations, a milling process (with high rotating

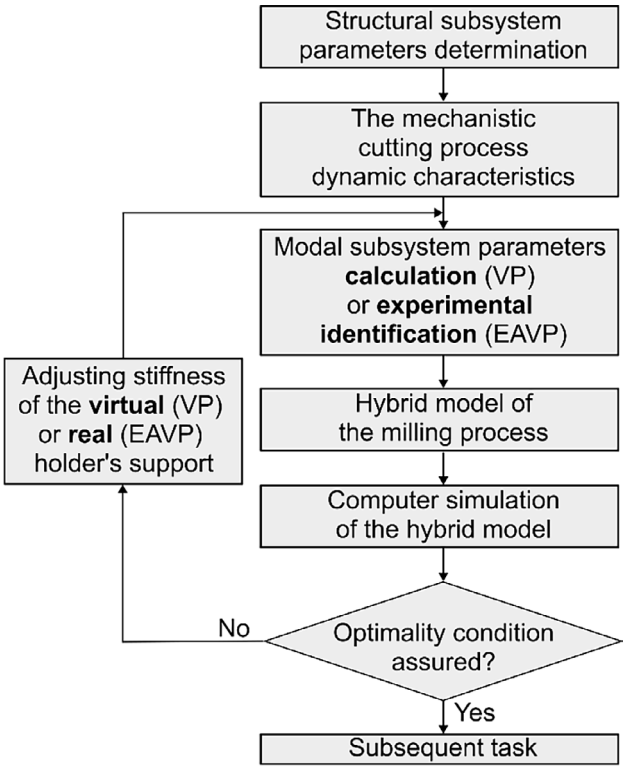

Figure 1. Common scheme for vibration suppression prototyping in milling flexible details

cutting tool) will be actually implemented using the generated tool paths and the determined cutting parameters, i.e., spindle speed, feed rate, cutting depth.

The proposed machining process implementation eliminates the need for a CAM postprocessor to modify machining parameters, unlike in previous studies [7]. All responsibility for reducing the level of vibration between the tool and the workpiece in the cutting process lies with a holder having adjustable support stiffness.

The portable test stand, used in the EAVP, will now be installed in the actual milling process. Research on the target system will enable:

- performance of the tool-flexible workpiece vibration suppression system using workpiece holder with adjustable support stiffness on a selected milling machine;
- final assessment of the vibration suppression efficiency in real milling process.

Computational model

Cutting process dynamics

To determine the best conditions for clamping the workpiece in a holder with adjustable stiffness simulations of the milling process are conducted. In the present case, the workpiece is flexible, while the tool is a slender ball-end mill. The milling process dynamic is analyzed (Figure 2) based on the assumptions outlined in [36]. The key assumptions are as follows:

- The tool rotates at spindle speed n, while the workpiece advances at feed rate v_f.
- Only the tool is modelled as a deformable finite element of the Euler-Bernoulli bar type (E-BB, [7]) with its upper end fixed, and the flexible workpiece in the form of a thin rectangular plate, clamped in a holder with adjustable stiffness (spring-damping element (SDE, [7, 37])). Other components of the milling machine structure are neglected [36, 38].
- The plate flexible workpiece is modelled using the rigid finite element method [37], incorporating the theory of thin bending plates [39].
- Proportional and delayed feedback due to the current and previous cutting edge passes along the cutting layer is considered, thus accounting for the effects of internal and external layer thickness modulation [7].
- At conventional tool edge-workpiece contact points, coupling elements (CEs) are located, which model the dynamics of the cutting process [7, 36]. Their positions relative to the workpiece vary with time as the tool rotates

at speed n. The instantaneous position of cutting edge no. l is described by the immersion angle $\varphi_l = \varphi(t)$, corresponding to the temporary position of CE no. l. The edges in contact with the material at a given moment are called "active" edges.

Other symbols appearing in Figure 2 are as follows:

- γ_0 – rake angle and α_0 – relief angle, as descriptors of geometry of the cutting edge,
- α_p – nominal depth of cut,
- F_{yl1}, F_{yl2}, F_{yl3} – cutting forces acting in the direction of the nominal cutting speed v_c, cutting layer thickness h_l and current depth of cut a_{pl}, respectively,
- D – tool trace diameter and milling widths B_1 and B_2,
- local rotating coordinate system x_{e1}, x_{e2}, x_{e3} of E-BB no. e,
- conventional tool-workpiece contact point S [7, 34, 36] and non-rotating coordinate system x_1, x_2, x_3 for this point, which moves linearly relative to the workpiece.

For the temporary point of the tool edge in contact with the workpiece, modelled as CE no. l, a proportional model of the cutting process dynamics was adopted [36]:

$$F_{yl1}(t) = \begin{cases} k_{dl} a_{pl}(t) h_l(t), & h_l(t) > 0 \wedge a_{pl}(t) > 0, \\ 0, & h_l(t) \le 0 \vee a_{pl}(t) \le 0, \end{cases} \quad (1)$$

$$F_{yl2}(t) = \begin{cases} \mu_{l2} k_{dl} a_{pl}(t) h_l(t), & h_l(t) > 0 \wedge a_{pl}(t) > \\ 0, & h_l(t) \le 0 \vee a_{pl}(t) \le \end{cases} \quad (2)$$

$$F_{yl3}(t) = \begin{cases} \mu_{l3} k_{dl} a_{pl}(t) h_l(t), & h_l(t) > 0 \wedge a_{pl}(t) > \\ 0, & h_l(t) \le 0 \vee a_{pl}(t) \le \end{cases} \quad (3)$$

where:

$$a_{pl}(t) = a_p - \Delta a_{pl}(t) \quad (4)$$

$$h_l(t) = h_{Dl}(t) - \Delta h_l(t) + \Delta h_l(t - \tau_l), \quad (5)$$

where: a_p – desired depth of cut, $\Delta a_{pl}(t)$ – dynamic change in depth of cut for CE no. l, $h_{Dl}(t)$ – desired cutting layer thickness for CE no. l; $h_{Dl}(t) \cong f_z \cos\varphi_l(t)$, $\Delta h_l(.)$ – dynamic change in cutting layer thickness for CE no. l, k_{dl} – average dynamic specific cutting pressure for CE no. l, μ_{l2}, μ_{l3} – cutting force coefficients fo CE no. l, as quotients of forces F_{yl2} and F_{yl1} and forces

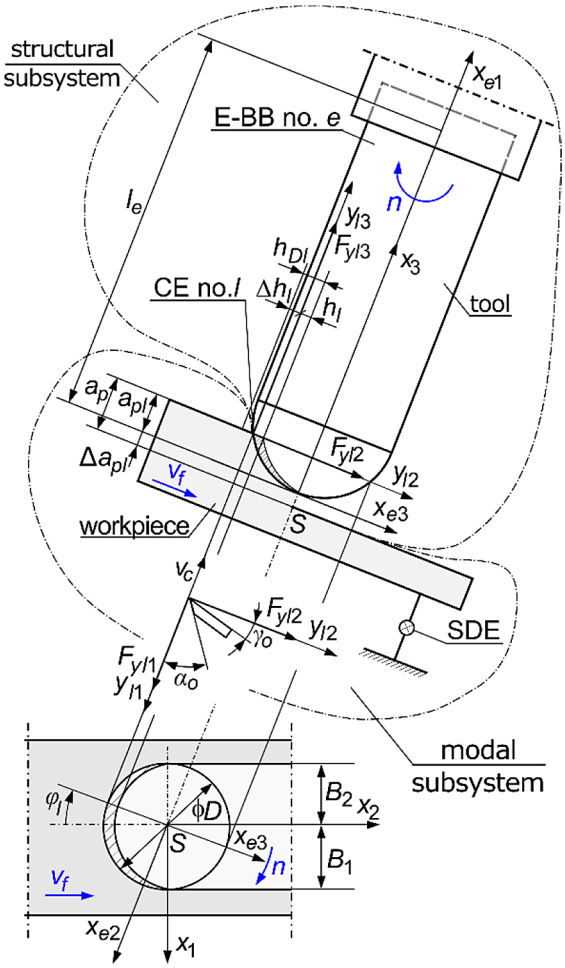

Figure 2. A scheme of a ball end milling process

F_{yl3} and F_{yl1}, τ_l – time delay between the same position of CE no. l and CE no. l-1, f_z – feed per tooth; $f_z = v_f/(nz)$, z – number of cutter teeth.

This model also considers the effects of internal and external layer thickness modulation and copes with the situation where the cutting edge loses contact with the workpiece.

The authors, informed by the experience of simulating the cutting processes of large-sized workpieces [36], also here decided on a practical approach based on a proportional mechanistic model, in which Equations 1–3 contain only three parameters: k_{dl}, μ_{l2} i μ_{l3}. Although these parameters lack direct physical interpretation, their carefully selected values ensure reliable simulation results, both with the VP and EAVP techniques.

The cutting forces corresponding to CE no. l in a 6-dimensional space are expressed as [36]:

$$\mathbf{F}_l(t) = \mathbf{F}_l^0(t) - \mathbf{D}_{Pl}(t)\Delta\mathbf{w}_l(t) + \mathbf{D}_{Ol}(t)\Delta\mathbf{w}_l(t - \tau_l), \quad (6)$$

where:

$$\mathbf{F}_l(t) = col(F_{yl1}(t), F_{yl2}(t), F_{yl3}(t), 0, 0, 0), \quad (7)$$

$$\mathbf{F}_l^0(t) = col(k_{dl}a_p h_{Dl}(t), \mu_{l2}k_{dl}a_p h_{Dl}(t), \mu_{l3}k_{dl}a_p h_{Dl}(t), 0, 0, 0), \quad (8)$$

$$\mathbf{D}_{Pl}(t) = \begin{bmatrix} 0 & k_{dl}\left(a_p - \Delta a_{pl}(t)\right) & k_{dl}h_{Dl}(t) & \\ 0 & \mu_{l2}k_{dl}\left(a_p - \Delta a_{pl}(t)\right) & \mu_{l2}k_{dl}h_{Dl}(t) & \mathbf{0}_{3\times3} \\ 0 & \mu_{l3}k_{dl}\left(a_p - \Delta a_{pl}(t)\right) & \mu_{l3}k_{dl}h_{Dl}(t) & \\ & \mathbf{0}_{3\times3} & & \mathbf{0}_{3\times3} \end{bmatrix}, \quad (9)$$

$$\mathbf{D}_{Ol}(t) = \begin{bmatrix} 0 & k_{dl}\left(a_p - \Delta a_{pl}(t)\right) & 0 & \\ 0 & \mu_{l2}k_{dl}\left(a_p - \Delta a_{pl}(t)\right) & 0 & \mathbf{0}_{3\times3} \\ 0 & \mu_{l3}k_{dl}\left(a_p - \Delta a_{pl}(t)\right) & 0 & \\ & \mathbf{0}_{3\times3} & & \mathbf{0}_{3\times3} \end{bmatrix}, \quad (10)$$

$$\Delta\mathbf{w}_l(t) = col\left(q_{zl}(t), \Delta h_l(t), \Delta a_{pl}(t), 0, 0, 0\right), \quad \Delta\mathbf{w}_l(t-\tau_l) = col(q_{zl}(t-\tau_l), \Delta h_l(t-\tau_l), \quad (11)$$

$$\Delta a_{pl}(t-\tau_l), 0, 0, 0) \quad (12)$$

where: $q_{zl}(t)$ – the relative displacement of the cutting edge and the workpiece along the y_{l1} direction at time t and $q_{zl}(t-\tau_1)$ – the relative displacement of the cutting edge and the workpiece along the y_{l1} direction at time $t-\tau_l$.

Relations (9) and (10) also take into account the geometric nonlinearity resulting from the dynamic change in depth of cut.

Modeling a flexible workpiece

Creating a discrete rigid finite element model of a workpiece in the form of a uniform thin bending plate with dimensions $L\times B\times h$ (Figure 3, h – plate thickness) involves isolating a finite number of rigid bodies (rigid finite elements, RFEs) describing kinetic energy storage, and a finite number of massless spring-damping elements (SDEs) describing strain energy storage and energy dissipation [37]. Each RFE has three degrees of freedom, i.e., a displacement in the direction normal to the plate surface and two angles of rotation about the axes of a rectangular coordinate system lying in the plate plane. The method for determining the SDEs (stiffness coefficients) and RFEs (inertia coefficients) parameters is presented in Appendix A1 and Appendix A2, respectively.

Additionally, the model included the masses of two vibration measurement sensors permanently mounted on the plate. Assuming the sensor positions S1 and S2, their masses were distributed evenly and concentrated at the centers of mass of adjacent RFEs. As a result, the masses of previously created RFEs no. 20 and 33, as well as 15 and 28, were increased without changing their mass moments of inertia. The presence of a holder with adjustable stiffness was also taken into account, whose moving mass in a direction perpendicular to the plate surface (see section 'A stand for testing the workpiece and the milling process'), was divided into RFEs 65, 13, 26, 39, 52, and 78. Here, too, the concentrated masses of these RFEs were increased without changing their mass moments of inertia. The stiffness coefficient of SDE (Figure 2) in the direction normal to the plate surface was distributed among the specified RFEs, as was the mass of the moving part of the holder.

This resulted in a computational model with 90 RFEs (270 degrees of freedom) and 286 SDEs. The model was subjected to calculations of *mod* natural frequencies and normal

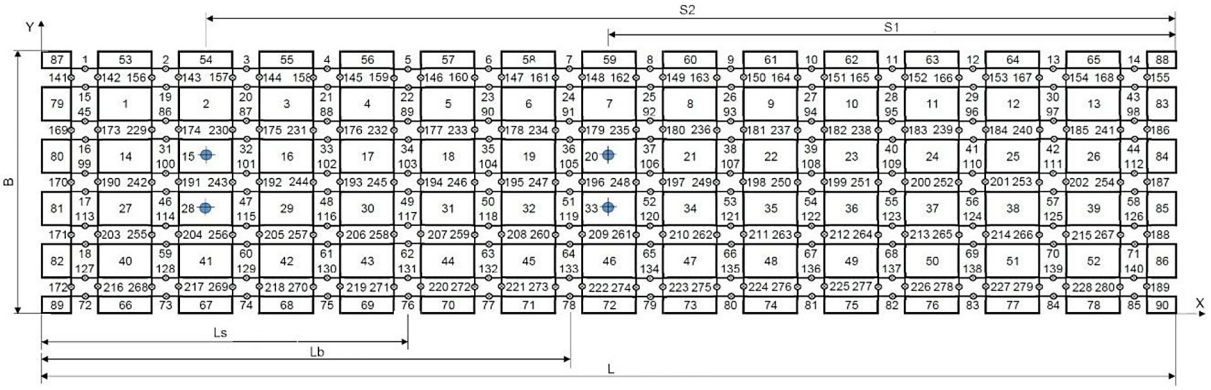

Figure 3. Division of a flexible rectangular plate into RFEs and SDEs

modes, $f_i^a, \boldsymbol{\Psi}_i^a, i = 1, \ldots, mod$. The proprietary APARA1, AMASTA and AWLS8 software were used to create the computational model and then calculate the natural vibrations. Both programs were developed in FORTRAN using the free 64-bit MSYS2 MinGW64 Shell toolkit and the free GNU compiler. The results of the natural vibration normal modes calculations were analyzed using MATLAB 2017 and 2022.

Hybrid model of the cutting process

The dynamics of the milling process is modelled using a hybrid system (Figure 2), which integrates modal and structural subsystems interconnected through coupling elements. The modal subsystem represents a flexible workpiece mounted in a stiffness-adjustable holder and moving at a feed rate v_f. It is described by its modal coordinate vector **a**. The following modal model parameters are identified:

- at the computational modal analysis stage – the frequencies and M-orthonormal modes of natural vibrations $f_i^a, \boldsymbol{\Psi}_i^a, i = 1, \ldots, mod$;
- at the experimental modal analysis stage – the natural frequencies and dimensionless damping coefficients $f_i^e, \zeta_i^e, i = 1, \ldots, mod$.

Considering a finite number *mod* of normal modes, the dynamic model of the workpiece is described as follows [7]:

- at the stage of computational modal analysis – $\boldsymbol{\Omega} = \mathrm{diag}(2\pi \mathrm{f}_\mathrm{i}^\mathrm{a})$, i = 1, …, *mod*, $\boldsymbol{\Psi} \equiv \boldsymbol{\Psi}^{\boldsymbol{a}} = [\boldsymbol{\Psi}_1^a \quad \ldots \quad \boldsymbol{\Psi}_{mod}^a]$. However, the elements $\zeta_\mathrm{i}^\mathrm{a}$, i = 1, …, *mod*, of the dimensionless damping coefficients' matrix $\mathbf{Z} = diag(\zeta_i)$, due to the lack of reliable analytical relationships, are roughly estimated;
- at the stage of experimental modal analysis – $\boldsymbol{\Omega} = \mathrm{diag}(2\pi \mathrm{f}_\mathrm{i}^\mathrm{a})$, i = 1, ..., *mod*, $\mathbf{Z} = \mathrm{diag}(\zeta_\mathrm{i}^\mathrm{e})$ i = 1, ..., *mod*, $\boldsymbol{\Psi} \equiv \boldsymbol{\Psi}^a$. Due to the insufficient number of sensors, which prevents precise identification of the normal mode, the appropriate normal modes determined at the stage of computational modal analysis were included.

The structural subsystem is a whirling slender ball end cutter. Its displacements are expressed by the vector of generalized coordinates **q** in the Cartesian system x_{e1}, x_{e2}, x_{e3}, which is fixed in one of the nodes of E-BB and rotates together with the cutter. Then these displacements are transformed to immovable coordinate system x_1, x_2, x_3. Therefore, the dynamics of the whirling slender tool is described by matrices of inertia $\mathbf{M}_\mathbf{e}$, damping $\mathbf{L}_\mathbf{e}$, and stiffness $\mathbf{K}_\mathbf{e}$ [7], as well as by the matrices resulting from the tool rotation, i.e. $\hat{\mathbf{L}}_e$ and $\widehat{\mathbf{K}}_e$ [7]. The way of defining the matrices $\hat{\mathbf{L}}_e$ and $\widehat{\mathbf{K}}_e$ of E-BB no. e, is shown in the Appendix A3.

With reference to the presented considerations, the matrix equation of the non-stationary model of the milling process in hybrid coordinates was obtained, i.e. (13), where: $\boldsymbol{\xi} = \begin{Bmatrix} \mathbf{q} \\ \mathbf{a} \end{Bmatrix}$ – hybrid coordinate vector of the hybrid system, $\mathbf{T}_l$ – transformation matrix of the displacement vector **q** from coordinates x_{e1}, x_{e2}, x_{e3} of E-BB no. *e*, to the coordinate system y_{l1}, y_{l2}, y_{l3} of CE no. *l* [36], $\mathbf{W}_l(t)$ – transformation matrix between the displacement vector in modal coordinates **a**, and the displacements in the coordinate system y_{l1}, y_{l2}, y_{l3} of CE no. *l* [36], i_l – number of "active" CEs.

Equation 13 is used to simulate non-stationary cutting process in the time domain. During the process, a continuous change in the geometrical position of the instantaneous points of contact between the tool and the workpiece is observed. However, it looks different than in the previous studies [7, 34]. This time, the position of CE no. l is invariant with respect to the rotational system x_{e1}, x_{e2}, x_{e3} of E-BB no. e, which results in constant elements of the matrix $\mathbf{T}_l$. To simulate the hybrid model of flexible workpiece milling, authorial AMATSUURA software, developed in the FORTRAN language (free 64-bit MSYS2 MinGW64 Shell toolkit and free

$$\begin{bmatrix} \mathbf{M}_e & \mathbf{0} \\ \mathbf{0} & \mathbf{I} \end{bmatrix} \ddot{\boldsymbol{\xi}} + \begin{bmatrix} \mathbf{L}_e + \hat{\mathbf{L}}_e - \hat{\mathbf{L}}_e^T & \mathbf{0} \\ \mathbf{0} & 2\mathbf{Z}\boldsymbol{\Omega} \end{bmatrix} \dot{\boldsymbol{\xi}} + \begin{bmatrix} \mathbf{K}_e - \widehat{\mathbf{K}}_e + \sum_{l=1}^{i_l} \mathbf{T}_l^T \mathbf{D}_{Pl}(t) \mathbf{T}_l & -\sum_{l=1}^{i_l} \mathbf{T}_l^T \mathbf{D}_{Pl}(t) \mathbf{W}_l(t) \\ -\sum_{l=1}^{i_l} \mathbf{W}_l^T(t) \mathbf{D}_{Pl}(t) \mathbf{T}_l & \boldsymbol{\Omega}^2 + \sum_{l=1}^{i_l} \mathbf{W}_l^T(t) \mathbf{D}_{Pl}(t) \mathbf{W}_l(t) \end{bmatrix} \boldsymbol{\xi} = \begin{bmatrix} \sum_{l=1}^{i_l} \mathbf{T}_l^T \mathbf{F}_l^0(t) + \mathbf{T}_l^T \mathbf{D}_{Ol}(t) \Delta \mathbf{w}(t - \tau_l) \\ -\sum_{l=1}^{i_l} \mathbf{W}_l^T(t) \mathbf{F}_l^0(t) - \mathbf{W}_l^T(t) \mathbf{D}_{Ol}(t) \Delta \mathbf{w}(t - \tau_l) \end{bmatrix}, \tag{13}$$

GNU compiler) was applied. On the other hand, the MATLAB 2017 and 2022 packages were used to analyze the results obtained.

2-dimensional interpolation

During the milling process, the tool moves along the workpiece, passing through successive regions dominated by different vibration modes. Thanks to computational modal analysis (subsection Modeling a flexible workpiece), the modal parameters of the workpiece are determined. However, they are identified only at the locations of the centers of mass of the RFEs. For simulations using hybrid models, it is necessary to specify normal modes for each point of calculation. In other words for a point with coordinates ξ_l, η_1 lying between the known positions of the scattered centers of mass at points (ξ_l, η_1), (ξ_{j2l}, η_{j1l}), (ξ_{j1l}, η_{j2l}) and (ξ_{j2l}, η_{j2l}) (Figure 4), the normal odes components must be determined. For this purpose, an adaptation of the 2-dimensional linear interpolation technique of normal modes is proposed. For a position lying between the locations where normal mode no. i, i = 1, ..., mod, is defined (i.e. between the centers of mass of appropriate RFEs), the component of the mode in the direction normal to the plate surface $\widehat{\Psi}_i$ is calculated according to the following formula (14).

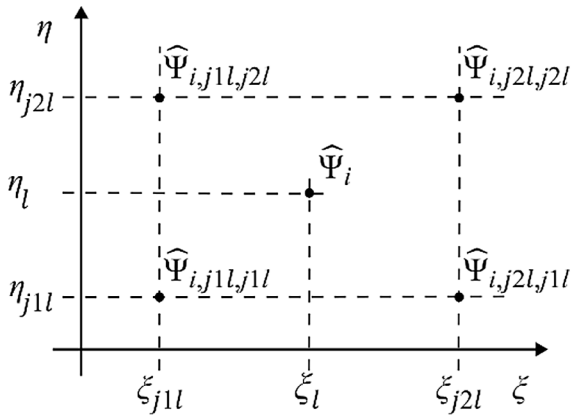

Figure 4. 2-dimensional interpolation of the normal mode component $\widehat{\Psi}_i$

$$\widehat{\Psi}_i(\xi_l, \eta_l) = [1 \quad \xi_l \quad \eta_l \quad \xi_l \eta_l] \begin{bmatrix} 1 & \xi_{j1l} & \eta_{j1l} & \xi_{j1l}\eta_{j1l} \\ 1 & \xi_{j2l} & \eta_{j1l} & \xi_{j2l}\eta_{j1l} \\ 1 & \xi_{j1l} & \eta_{j2l} & \xi_{j1l}\eta_{j2l} \\ 1 & \xi_{j2l} & \eta_{j2l} & \xi_{j2l}\eta_{j2l} \end{bmatrix}^{-1} \begin{Bmatrix} \widehat{\Psi}_{i,j1l,j1l} \\ \widehat{\Psi}_{i,j2l,j1l} \\ \widehat{\Psi}_{i,j1l,j2l} \\ \widehat{\Psi}_{i,j2l,j2l} \end{Bmatrix}. \tag{14}$$

In this way, the transformation matrix appearing in equation (13) also becomes dependent on the location of the current point, i.e.:

$$\mathbf{W}_l\left(t, \xi_l(t), \eta_l(t)\right) = \begin{bmatrix} \mathbf{\Theta}_l(t)_{3\times3} & \mathbf{0}_{3\times3} \\ \mathbf{0}_{3\times3} & \mathbf{\Theta}_l(t)_{3\times3} \end{bmatrix} \mathbf{C}_W \widehat{\mathbf{\Psi}}\left(\xi_l(t), \eta_l(t)\right), \tag{15}$$

whereby:

$$\mathbf{\Theta}_l(t) = \begin{bmatrix} \cos\varphi_l & -\sin\varphi_l & 0 \\ \sin\varphi_l & \cos\varphi_l & 0 \\ 0 & 0 & 1 \end{bmatrix}, \tag{16}$$

$$\mathbf{C}_W = col(0,0,1,0,0,0), \tag{17}$$

$$\widehat{\mathbf{\Psi}}\left(\xi_l(t), \eta_l(t)\right) = \begin{bmatrix} \widehat{\Psi}_1(\xi_l, \eta_l) \\ \vdots \\ \widehat{\Psi}_i(\xi_l, \eta_l) \\ \vdots \\ \widehat{\Psi}_{mod}(\xi_l, \eta_l) \end{bmatrix}^T. \tag{18}$$

Using the same approach, it is also possible to extrapolate normal modes to points beyond the centers of mass of the RFEs located on boundaries of the discrete workpiece model. Interpolation of the simulated model based on the rigid finite element method is performed during the execution of the previously mentioned proprietary AMATSUURA software.

Summary of the method

The proposed method responds to the important need for computational simulation of the entire ball end milling cutter machining, taking into account the thin rectangular workpiece, the slender cutting tool and the dynamics of the cutting process, as well as the non-stationary and non-linear vibration state. In comparison to the previous research, this method has now been substantially modified. This includes:

- modeling the flexible workpiece using the rigid finite element method, which eliminates

the need for often unavailable and expensive FEM software;
- creating a modal model of the workpiece mounted in a stiffness-adjustable holder, while simultaneously utilizing computational and experimental modal analysis;
- consideration of the influence of the spindle speed of the rotary tool on its dynamic characteristics. In contrast to the axially symmetrical, non-rotating tool (this one exhibits double natural frequencies and decoupled modes in two mutually perpendicular planes), two distinct frequencies and corresponding coupled modes of vibration are now detected.

This modified method offers a higher level of accuracy in simulating the non-stationary model of the milling process with slender tools, enabling significantly improved prediction of the best and worst conditions for clamping flexible small-sized workpieces.

The matrix equation of dynamics (13), which is the basis for the use of VP and EAVP techniques, is transparent and at the same time necessary, because it describes a non-stationary and nonlinear system in hybrid coordinates. It is solved in the time domain by the Newmark numerical integration method [40], under known initial conditions. A possible simplification of this seemingly complicated mathematical description would result in the need to omit important properties of the analyzed milling process. And the authors wanted to take them into account. Otherwise, in addition to the above-mentioned new modifications, it would be necessary to omit e.g.: variable system configuration, cutting process dynamics, separation of stationary (modal) and non-stationary (structural) subsystems.

RESULTS

A stand for testing the workpiece and the milling process

Two flexible workpieces in the form of thin rectangular plates with dimensions 175 × 50 × 5 mm (flatness deviations of 5 μm measured on a ZENITH 3 measuring machine with a resolution of ±2 μm) made of bronze CC331G and aluminum alloy EN AW-6101 A, respectively, were selected for the experimental tests. Each workpiece was clamped in a holder with adjustable stiffness, which in turn was mounted on the table of a 5-axis CNC machining center MATSUURA MX 520 (n_{max} = 20,000 rpm). Next, sensors (PCB accelerometers) were placed: no. 0 (measuring range ±100 g) – on the moving part of the holder, no. 1 and 2 (measuring ranges ±250 g) – on the underside of the workpiece, at a distance of 70 and 127 mm, respectively, from the movable part of the holder (Figure 5). The purpose of them is to measure signals (sampling frequency 10 kHz) stimulated using a 086C03 PCB modal hammer, and in the case of sensor 1 – additionally to measure vibrations during the milling process.

For modal tests, 10 impacts (H3 estimator) were performed with a 2 second impact recording time. Signals were measured using NI PXI 4496 dynamic signal acquisition card installed in PXI 8861 real-time controller. For this purpose, appropriate proprietary software for data processing in the NI LabView RT environment was launched.

The operating principle of a holder with adjustable stiffness is as follows (Figure 5b). The movable part, along with the mounted workpiece, can move vertically relative to the immovable part thanks to a sliding kinematic pair. Additionally, the workpiece deflects relative to the point of restraint in the holder. The stiffness coefficient of the vertical kinematic pair depends on the support location of the flexible beam, which can be changed by adjusting the micrometer screw. Therefore, different screw settings change the natural vibration frequency of the workpiece in the holder, under different and repeatable clamping conditions. The latter significantly affects the level of relative vibration of the tool-to-workpiece during milling.

On each workpiece (top surface of the plate), 6 grooves of 25 mm length (from L_b = 80 to L_s = 55 mm from the free end, Figure 3) were made as normal milling with a slender ball end milling cutter FETTE EBG R16.016AN160 (length 160 mm, ϕ16h6 i.e. $\phi 16^{+0,000}_{-0,011}$) equipped with an insert having 2 cutting edges. The milling cutter was clamped in a SCHUNK 206 436 ϕ20 3415 hydraulic chuck in such a way that the radial run-out of the tool in the chuck was 0.010 mm and the length of the free part after clamping was 120 mm. Identical cutting parameters were assumed for all tool passes, i.e. tool rotational speed n = 15,000 rpm, feed rate v_f = 300 mm/min and nominal cutting depth a_p = 0.1 mm. The considerable rotational speed of the tool justifies taking into account the influence of the speed on the rotating subsystem's dynamic features.

Ball end milling of thin plate of bronze CC331G

Computational modal analysis

The computational model of the thin rectangular plate CC331G was created according to the method described in subsection Modeling a flexible workpiece, assuming the following data: $\rho = 7.6 \times 10^3$ kg/m^3, $E = 1.3 \times 10^{11}$ Pa, $G = 4.89 \times 10^{10}$ Pa, $\nu = 0.33$.

Furthermore, mass of the movable part of the adjustable vertical holder was assumed to be 2 kg. The vertical stiffness coefficient of the holder (SDE, Figure 2) was determined by performing a modal test of the holder itself (without the workpiece) and measuring natural frequencies for various micrometer screw settings. This is justified by the fact that the mass of the movable part, together with spring support, constitutes on oscillator with one degree of freedom. The relevant results are presented in Table 1.

As a result of the performed calculations, the natural frequencies and normal modes, $f_i^a, \Psi_i^a, i = 1, \ldots, mod$, were determined, and only those modes for which f_i^a does not exceed 1000 Hz (i.e. for $mod = 3$) were taken into account. The calculated frequencies (especially for mode 1) significantly depend on the micrometer screw setting (Table 2). However, the calculated modes, illustrated as example for the 23 mm setting (Figure 6), are very similar also for other screw settings. Thus, mode 1 results from the dominant role of the holder flexibility. Modes 2 and 3, on the other hand, are the bending modes of the plate, where mode 2 has one, and mode 3 – two node lines in the direction of the plate width.

Virtual prototyping

Virtual prototyping (VP) involves simulating a computational model of the milling process (section 'A stand for testing the workpiece and the milling process') using a slender ball end cutter on a flexible rectangular plate-shaped workpiece. The extremely unfavorable case of chisel cutting was selected (cutter axis normal to the machined surface). The parameters of the workpiece modal model, i.e., f_i^a, Ψ_i^a, $i = 1, ..., 3$, were determined in subsection 'Computational modal analysis', but due to the lack of reliable analytical relationships, the values $\zeta_i^a = 0.01, i = 1, \ldots, 3$ were estimated as the same. The abstract dynamic parameters of the cutting process were used

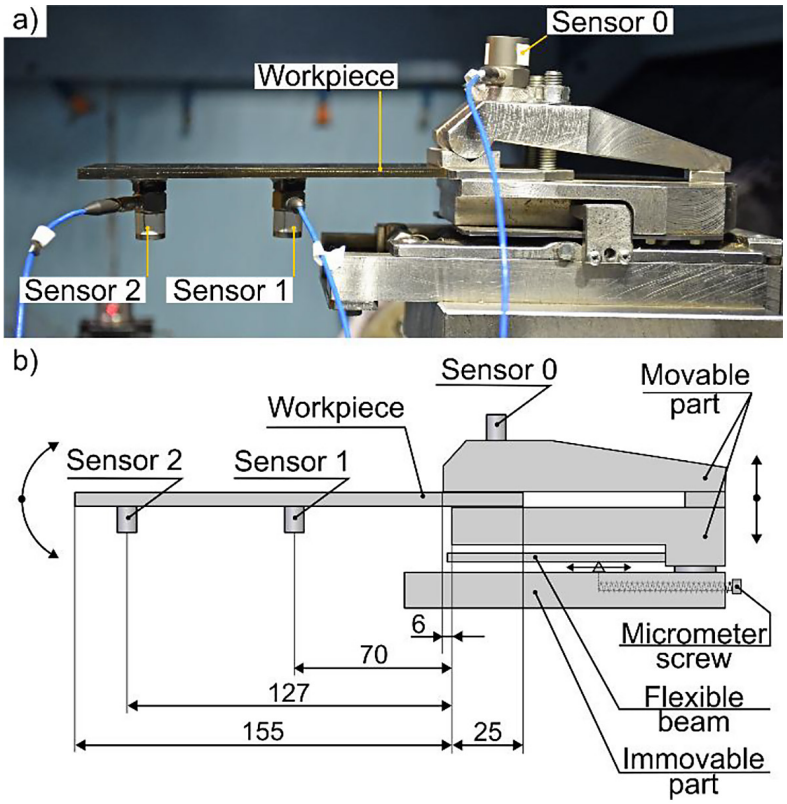

Figure 5. An adjustable vertical holder: a) overall view, b) important items of the structure

for the simulation: k_{dl} = 140 daN/mm², μ_{l2} = 0.4, μ_{l3}= 0.4 and 0.51. The basis for the selection was the highest value of k_{dl}, at which the result of the simulation was numerically stable. On the other hand, the adoption of two different values of μ_{l3} was aimed at better matching the RMS value of the vibrations of the simulated plot with the values measured during the ITS technique.

Already at this stage, a criterion for finding the best micrometer screw setting can be formulated. The desired setting corresponds to the lowest stiffness at which chatter vibration disappears. This phenomenon can be recognized by observing the amplitude spectrum. Thus, chatter vibration is accompanied by a single peak with a significantly dominant amplitude and a frequency close to one of the workpiece's natural vibration frequencies. As chatter vibration disappears, as a result of increasing the holder stiffness, many periodic and combined resonances occur [41], but with much smaller amplitudes. This is accompanied by a significant reduction in the RMS. Example results for μ_{l3} = 0.51 are illustrated in Figure 7.

Experimental modal analysis

In order to identify the dominant natural vibrations for various workpiece clamping, modal tests were conducted at 6 different micrometer screw settings, identical to those described in subsection Computational modal analysis.

Signals stimulated by striking the moving part of the holder near sensor S0 with a modal hammer were measured using sensors S0, S1 and S2. For the selected workpiece clamping configurations, frequency response functions (FRFs) and their corresponding coherence functions were determined (Figure 8). Three magnificent natural frequencies in the range up to 1000 Hz were then identified, along with their dimensionless damping coefficients (Table 3). Damping was identified based on the acceleration FRFs, using manual peak selection and subjective evaluation of the Hilbert transform results visualization. The FRF channel with the highest peak for a given frequency was selected for damping identification. Differences between values identified for the same mode, but based on data from different channels, reach up to ±20%. Therefore, the results are rounded to 2 significant digits.

The most reliable range for identifying the parameters of the modal model was when the coherence function exceeded 0.9. This approach ensures that the results obtained in individual tests are reproducible with identical micrometer screw settings and signal excitation and recording methods. This is the only way to assess the accuracy of the workpiece model mounted in the holder.

Table 1. Stiffness coefficients of adjustable vertical holder

Micrometer screw setting [mm]	Measured natural frequency [Hz]	Vertical stiffness coefficient [N/m]
23	114.5	1.035144×10^6
20	107.0	9.039768×10^5
15	88.5	6.184097×10^5
10	77.0	4.681351×10^5
5	65.5	3.387446×10^5
0	56.5	2.520500×10^5

Table 2. Computed natural frequencies of a set "adjustable vertical holder-flexible workpiece"

Micrometer screw setting [mm]	Natural frequency *f* [Hz]		
	1	2	3
23	98.45	140.80	806.17
20	93.34	138.77	806.14
15	79.10	135.47	806.08
10	69.47	134.20	806.04
5	59.50	133.32	806.02
0	51.52	132.80	806.00

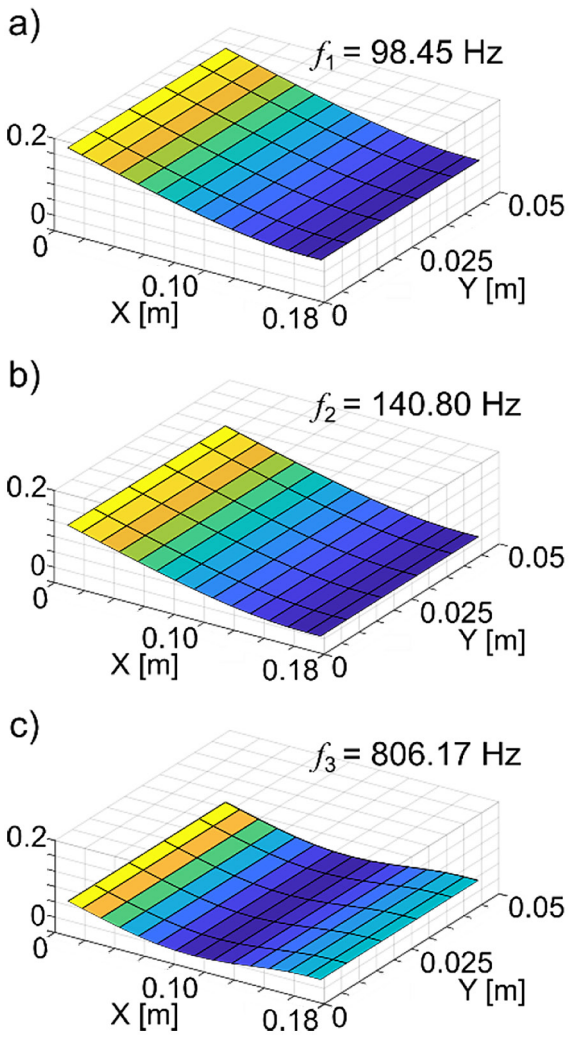

Figure 6. Exemplary results of the normal modes calculation, for screw setting 23 mm

Experimentally aided virtual prototyping

Some parameters of the workpiece modal model, i.e., $f_i^e, \zeta_i^e, i = 1, \ldots, 3$, were determined in subsection Experimental modal analysis, but due to the lack of ability to identify appropriate normal modes, the latter were assumed as identified in subsection Computational modal analysis, i.e. $\Psi \equiv [\Psi_1^a \quad \Psi_2^a \quad \Psi_3^a]$. The same abstract dynamic parameters of the cutting process, as in subsection Virtual prototyping, were adopted for the simulation: k_{dl} = 140 daN/mm^2, μ_{l2} = 0.4, μ_{l3} = 0.2 and 0.51.

Example results for μ_{l3} = and 0.51, at minimum and maximum holder stiffness, are shown (Figure 9). The simulatio results obtained using the VP and EAVP techniques are compared in Figure 10. It turned out that the simulation of the milling model at the parameters determined by the experimental modal analysis shows, in contrast to VP, small changes in the RMS of the workpiece vibration, depending on the change in the stiffness of the holder.

Experimental milling results

In order to successfully apply the mechatronic design technique based on the implementation in the target system (ITS) of the previously utilized VP and EAVP techniques, experimental studies were conducted on previously simulated normal milling passes with various stiffness settings of the fixture holding the flexible workpiece (Figure 11). For each groove, the RMS vibration displacements were measured using the closest sensor S1, and the obtained results were compared with the results of the VP and EAVP techniques (Figure 10). Surface roughness parameters obtained in different passes were also used to assess the accuracy of predicting the results of ball end milling of the flexible workpiece (Figure 12).

Ball end milling of thin plate of aluminum alloy EN AW-6101A

Computational modal analysis

The computational model of a thin rectangular plate of aluminum alloy EN AW-6101A was created, similarly to the case of bronze CC3331G (subsection 'Computational modal analysis'), according to the method described in subsection 'Modeling a flexible workpiece'. Following data was assumed: $\rho = 2.7 \times 10^3$ kg/m^3, $E = 7.0 \times 10^{10}$ Pa, $G = 2.61 \times 10^{10}$ Pa, $\nu = 0.34$. The vertical stiffness coefficients of the holder (SDE, Figure 2) are identical to those of the bronze CC3331G workpiece (Table 1).

Subsequently, the natural frequencies and normal modes $f_i^a, \Psi_i^a, i = 1, \ldots, mod$ were determined, and only those modes for which f_i^a does not exceed 1000 Hz (i.e. for mod = 3). Here, too, the calculated frequencies (especially for mode 1) depend greatly on the setting of the micrometer screw (Table 4). On the other hand, the calculated modes are very similar to those obtained in the case of bronze CC3331G (Figure 6). Hence, their illustrations were abandoned.

Experimental modal analysis

In order to identify the dominant natural vibrations for various workpiece clamping, modal

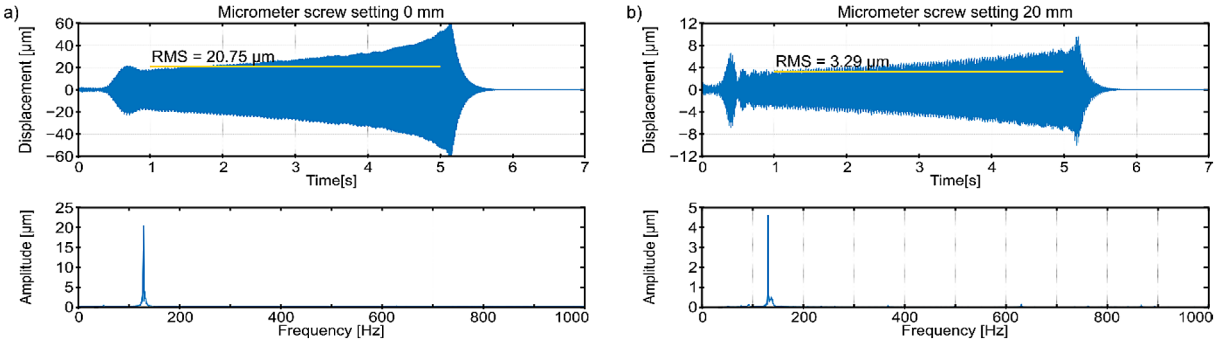

Figure 7. Time plots and amplitude spectra during ball end milling: a) presence of chatter vibrations, vibrations close to the plate free vibrations dominate, f = 129.76 Hz, b) a lack of chatter vibrations, combined resonance dominates, f = 131.70 Hz

Table 3. Measured natural frequencies and dimensionless damping coefficients of a set "adjustable vertical holder-flexible workpiece"

Micrometer screw setting [mm]	Natural frequency f [Hz]			Dimensionless damping coefficient ζ		
	1	2	3	1	2	3
23	90.50	108.00	621.00	0.011	0.011	0.011
20	87.50	105.00	620.00	0.013	0.030	0.010
15	79.00	99.00	620.00	0.011	0.017	0.010
10	66.00	97.50	619.50	0.009	0.009	0.010
5	55.00	96.50	617.50	0.025	0.007	0.010
0	45.50	96.00	617.50	0.028	0.035	0.010

tests were conducted at 6 different micrometer screw settings, identical to those described in subsection 'Computational modal analysis'.

For the selected workpiece clamping configurations, the frequency response functions (FRF) and the corresponding coherence functions were determined in the same manner as in subsection Experimental modal analysis (Figure 13). And then, three magnificent natural frequencies, whose values do not exceed 1000 Hz, were identified with their accompanying dimensionless damping factors (Table 5).

Mechatronic design techniques

Virtual prototyping (VP), which involves the simulation of an abstract computational model of the milling process (section 'A stand for testing the workpiece and the milling process') using a slender ball milling cutter on a flexible rectangular plate-shaped element, was carried out in a similar way to subsection Virtual prototyping. Modal parameters of the workpiece, i.e. $f_i^a, \boldsymbol{\Psi}_i^a, i = 1, \ldots, 3$, have been specified in subsection 'Computational modal analysis', but due to the lack of reliable analytical relationships, the values $\zeta_i^a = 0.01, i = 1, \ldots, 3$, have been estimated. The parameters of the cutting process were adjusted for the simulation: k_{dl} = 140 daN/mm^2, μ_{l2} = 0.4, μ_{l3} = 0.2. As in the case of bronze CC3331G, the basis for the selection was the highest value of k_{dl}, at which the result of the simulation was numerically stable.

For experimentally aided virtual prototyping (EAVP), some parameters of the workpiece modal model, i.e. $f_i^e, \zeta_i^e, i = 1, \ldots, 3$, were specified in subsection Experimental modal analysis, but due to the inability to identify the corresponding normal modes, the latter were adopted as specified in subsection Computational modal analysis, i.e. $\boldsymbol{\Psi} \equiv [\boldsymbol{\Psi}_1^a \quad \boldsymbol{\Psi}_2^a \quad \boldsymbol{\Psi}_3^a]$. The same abstract dynamic parameters of the cutting process, i.e. k_{dl} = 140 daN/mm^2, μ_{l2} = 0.4, μ_{l3} = 0.2 were used for the simulation.

The simulation results obtained using the VP and EAVP techniques are compared in Figure 14. It turned out that both simulated models of the milling process show a similar trend of reduction of RMS of the workpiece, along with an increase in the stiffness of the clamping in the holder.

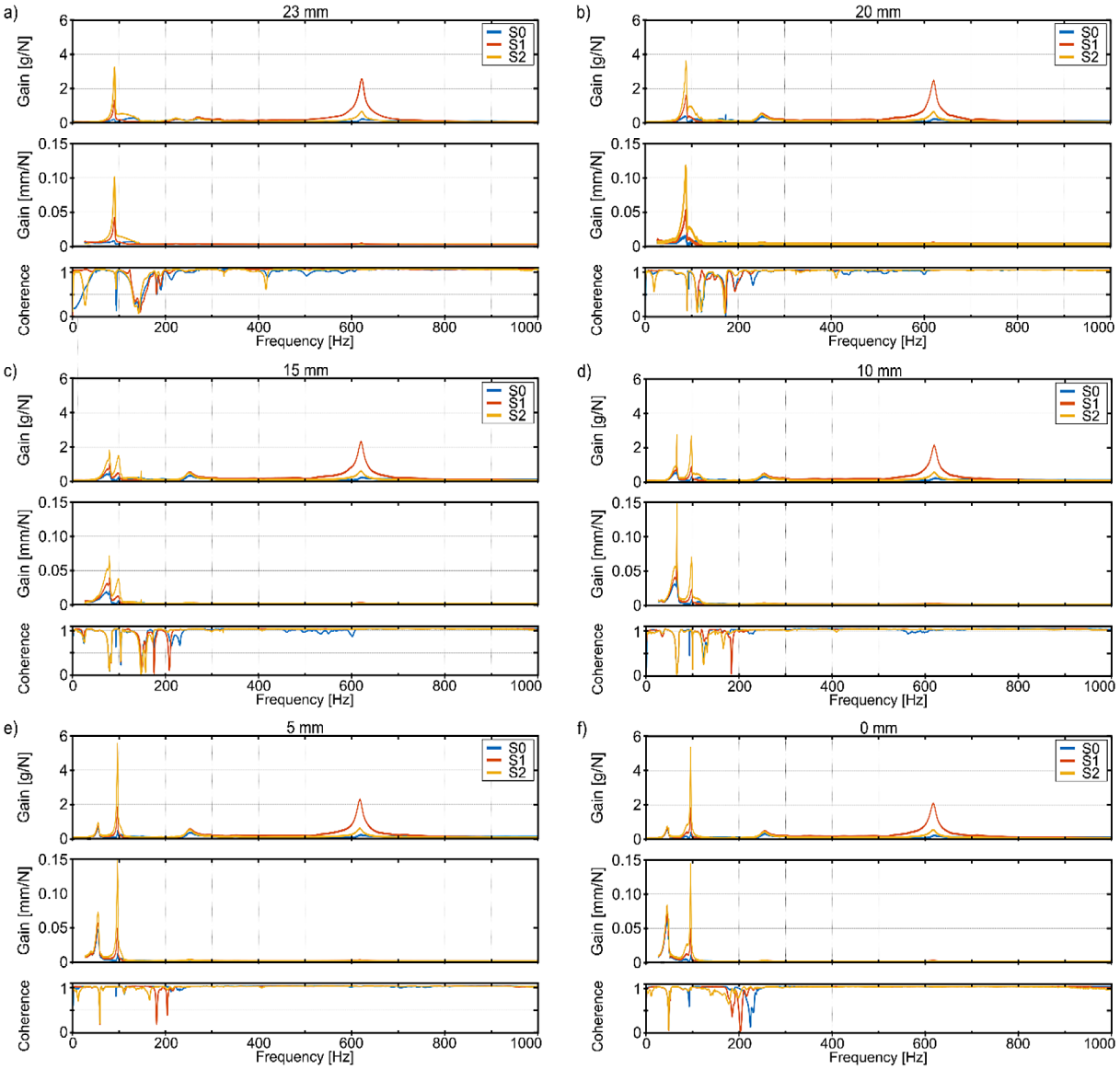

Figure 8. Frequency response functions (FRF) and coherence functions for different holder micrometer screw settings: a) 23 mm, b) 20 mm, c) 15 mm, d) 10 mm, e) 5 mm, f) 0 mm

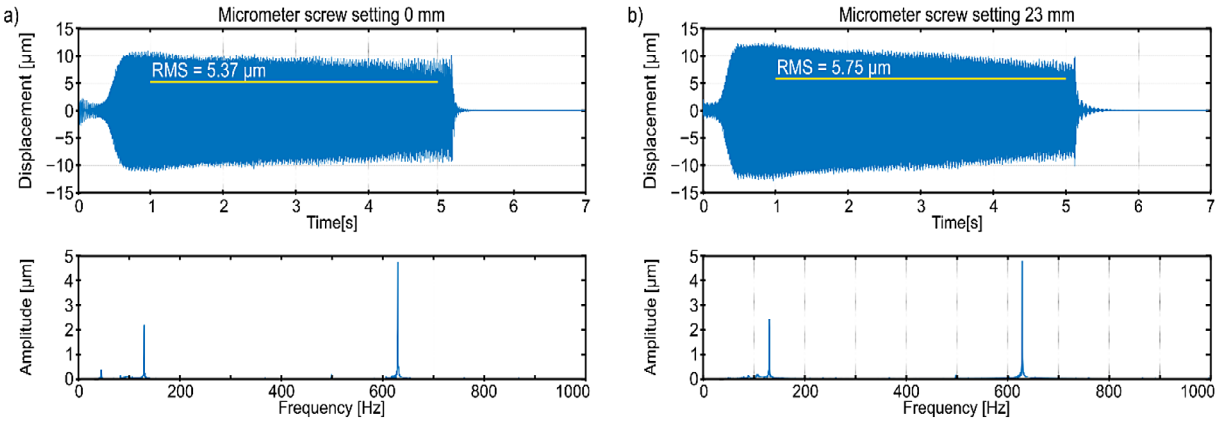

Figure 9. Time plots and amplitude spectra during ball end milling: a) minimum stiffness of adjustable holder, combined resonance f = 130.90 Hz, vibration close to natural frequency f = 630.90 Hz, b) maximum stiffness of adjustable holder, combined resonance f = 131.70 Hz, vibration close to natural frequency f = 631.28 Hz

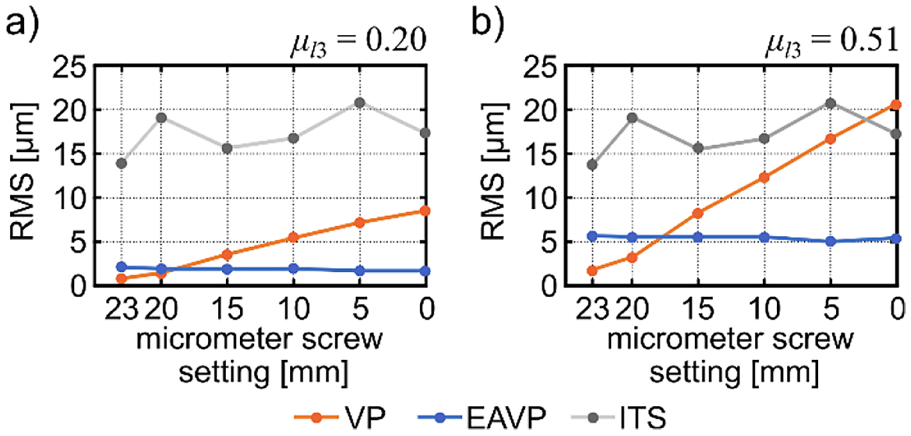

Figure 10. Comparison of RMS values obtained for various techniques of mechatronic design for: a) μ_{l3} = 0.2 and b) μ_{l3} = 0.51

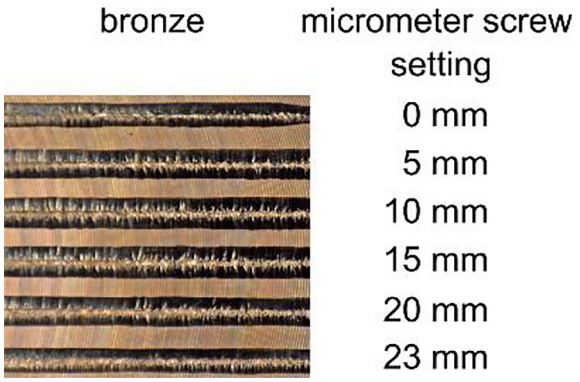

Figure 11. The results of ball end milling for various holder settings

Experimental milling results

In order to effectively apply the results of the VP and EAVP techniques used so far in the form of implementation in the target system (ITS), experimental studies were carried out on previously simulated normal milling passes (Figure 15). RMS vibration displacements were compared with the results of VP and EAVP techniques (Figure 14). For the purpose of assessing the accuracy of the prediction of results, the appropriate roughness parameters were measured as well (Figure 16).

DISCUSSION

The RMS measurement results during the ITS milling process of the CC331G bronze workpiece (14–20 µm) showed that the mechatronic design techniques used, i.e. VP and EAVP, generate different predictions, and the simulation results (especially for μ_{l3} = 0.2) are clearly underestimated. Thus, in the case of the VP technique, the successive stiffening of the workpiece in the holder (micrometric screw settings from 0 to 23 mm) results in a significant reduction in the RMS values of vibrations from approx. 9 to 1 µm (at μ_{l3} = 0.2) and from approx. 20 to 1.5 µm (at μ_{l3} = 0.51). On the other hand,

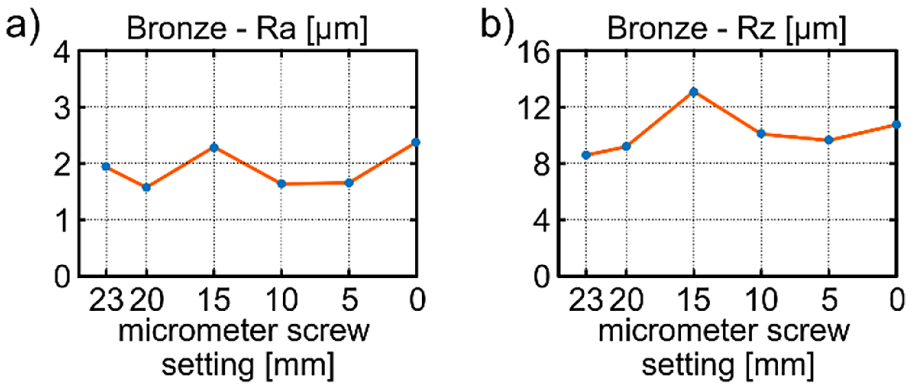

Figure 12. Roughness parameters for various holder settings

Table 4. Computed natural frequencies of a set of "adjustable vertical holder-flexible workpiece"

Micrometer screw setting [mm]	Natural frequency *f* [Hz]		
	1	2	3
23	107.218	147.686	905.912
20	100.879	146.679	905.901
15	84.309	145.141	908.876
10	73.635	144.573	905.862
5	62.792	144.175	905.851
0	54.233	143.944	905.844

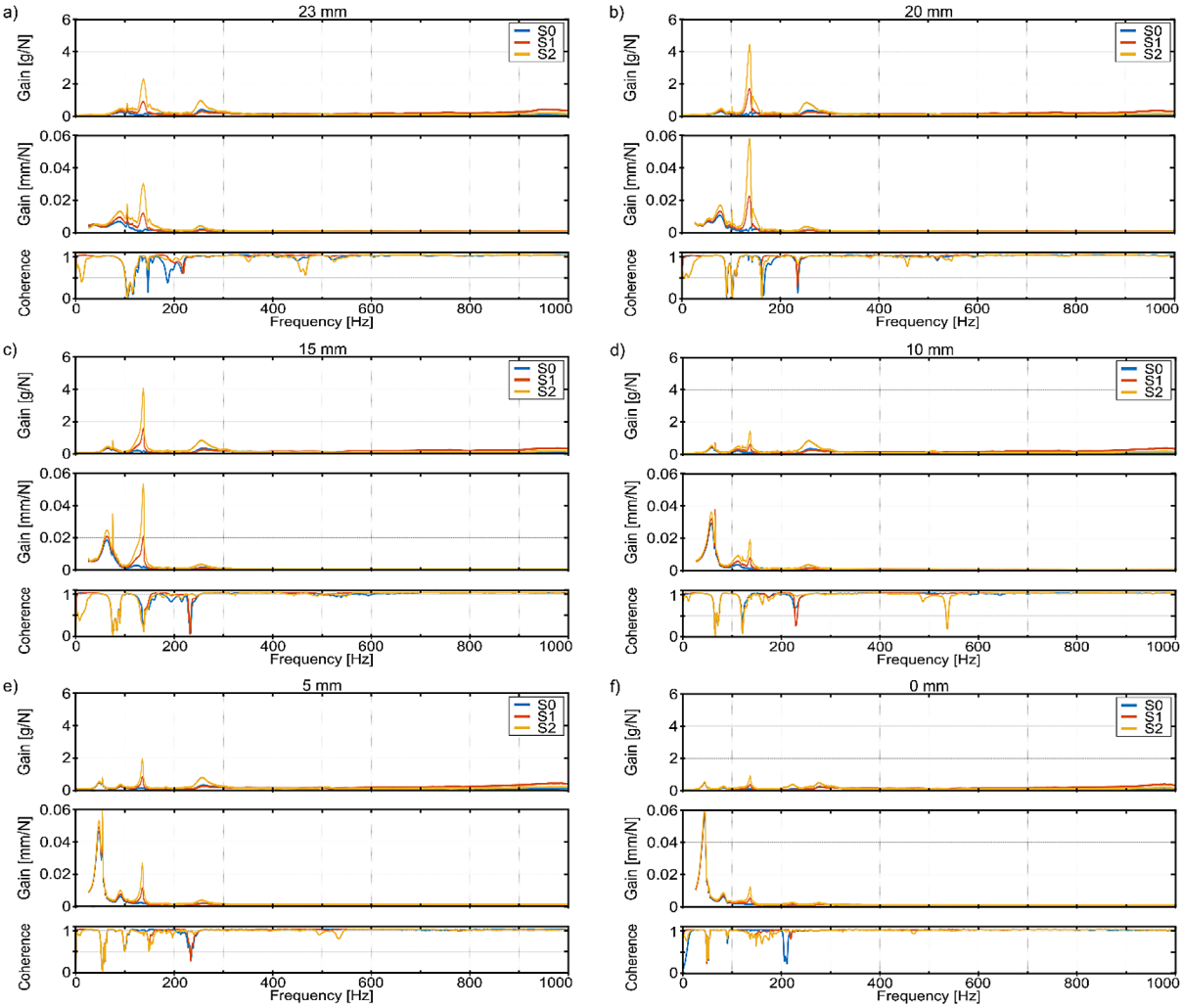

Figure 13. Frequency response functions (FRF) and coherence functions for different holder micrometer screw settings: a) 23 mm, b) 20 mm, c) 15 mm, d) 10 mm, e) 5 mm, f) 0 mm

in the case of the EAVP technique, the RMS value of vibrations remains practically unchanged and amounts to approx. 2 µm (at μ_{l3} = 0.2) and approx. 5 µm (at μ_{l3} = 0.51). Hence, it is proposed to intersect the VP and EAVP trend lines indicating the suggested best prediction (20 mm setting). Justification of such an approach is confirmed by the groove roughness parameters R_a and R_z obtained as a result of ITS, the values of which, for the suggested setting, do not exceed 1.5 and 9 µm, respectively. This classifies the surface quality obtained for this best setting even as close to grinding.

The results of RMS measurements during the ITS milling of an EN AW-6101A aluminum alloy workpiece (14–18 µm) showed that

Table 5. Measured natural frequencies and dimensionless damping coefficients of a set of "adjustable vertical holder-flexible workpiece"

Micrometer screw setting [mm]	Natural frequency *f* [Hz]			Dimensionless damping coefficient ζ		
	1	2	3	1	2	3
23	92.0	137.0	253.5	0.050	0.024	0.031
20	79.5	137.5	253.5	0.053	0.015	0.038
15	75.0	137.0	255.5	0.050	0.022	0.040
10	59.0	136.0	255.5	0.047	0.012	0.036
5	48.0	135.0	256.0	0.047	0.010	0.038
0	44.0	136.5	277.0	0.034	0.015	0.025

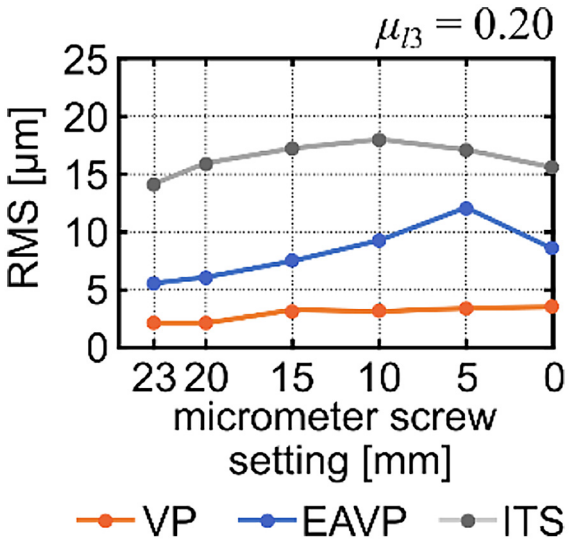

Figure 14. Comparison of RMS values obtained for various techniques of mechatronic design for $\mu_{I3} = 0.2$

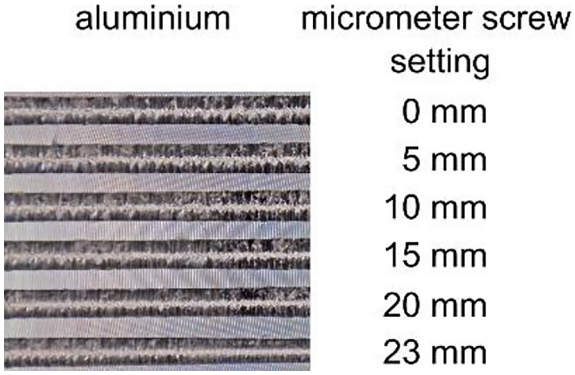

Figure 15. The results of ball end milling for various holder settings

both mechatronic design techniques, i.e. VP and EAVP, accurately predicted the best (screw adjustment 23 mm) and worst (screw adjustment 5–10 mm) setting. Although the simulated RMS values were slightly underestimated (2–4 μm at VP and 5–12 μm at EAVP), a consistent trend in the computer prediction was clearly observed. The simulation results did not fully confirm the obtained roughness parameters of the grooves, in the best case scenario, but the R_a and R_z values did not exceed 2.5 and 16 μm, respectively. This classifies the obtained surface quality as finishing machining.

CONCLUSIONS

The mechatronic design techniques proposed in this article, i.e. VP and EAVP, precisely meet the requirements for clamping a thin-walled flexible workpiece in a holder with adjustable stiffness. This was confirmed by comparing the trends in the RMS values calculated and recorded in the actual milling operation. Furthermore, there are two important advantages of the proposed methodology. First, access to licensed and expensive Finite Element Method software is not required to create a simulation of a specific computational model of the workpiece. Proprietary computational programs are sufficient to create and solve a rigid finite element method model. Second, the task of experimental modal analysis is limited to identifying only the natural frequencies and dimensionless damping coefficients for selected normal modes. For this purpose, minimal and significantly less expensive measurement equipment is sufficient. The latter contains only one modal hammer, a single accelerometer and a dual-channel data acquisition card.

The limitation of the proposed method is the requirement to develop a complicated calculational model and dedicated software for the milling simulation. This approach is not easy to implement in the workshop and is relatively time-consuming, although it has a solid substantive

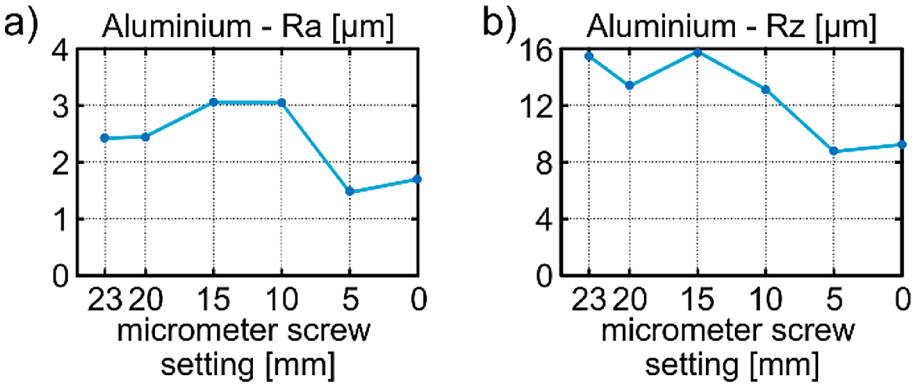

Figure 16. Roughness parameters for various holder settings

basis and a strong technical rationale. It demands advanced professional knowledge, specialized qualifications, and practical skills. However, its indisputable advantage is that it accurately predicts the best, and sometimes even the worst, variant of clamping the workpiece in a fixture with adjustable stiffness. The former is particularly important, especially in light of potential practical applications.

In addition to the above limitations, it is necessary to indicate the problem of numerical instability of the solution of the non-stationary strongly nonlinear equation of the dynamics of the milling process, resulting from the Newmark method of "step-by-step" integration. It is impossible to indicate an unambiguous scientific criterion of searching for the condition of stability of the solution. Hence, at the moment, the authors suggested choosing the largest value of the k_{dl} parameter, for which the solution of the calculation model of the milling process is numerically stable. Another limitation is the applicability of the proposed method to the case of bending vibrations of a thin plate. The reason for this is the insufficient number of sensors, which makes it impossible to identify the torsional modes of the plate. On the other hand, an important challenge is the search for a better compatibility of the natural vibration frequencies obtained with VP and EAVP, which the authors are currently working on. This is because the VP technique is the only source of knowledge about the normal modes, which are then used in the EAVP technique.

The deliverables of the paper will not be directly commercialized. However, these achievements may contribute to the refinement of the industrial version of the fixture with variable stiffness of thin-walled workpiece clamping, which could attract its commercialization in the future.

Funding

Financial support of these studies from Gdańsk University of Technology by the DEC-14/1/2022/IDUB/I3b/Ag grant, on "Development of a method for selecting the stiffness of a flexible workpiece clamping for vibration suppression during high-speed milling with slender tools" under the Argentum Triggering Research Grants – 'Excellence Initiative – Research University' program is gratefully acknowledged.

Acknowledgements

Material research on the MATSUURA MX 520 machining center were performed thanks to cooperation with the Hydromechanika Sp. z o.o. Sp. k., Ostaszewo, Poland.

REFERENCES

1. Sutter G, Chevrier P, Faure L, Petit B. Damages analysis of cutting tools in machining of titanium alloy (Ti6Al4V). International Journal of Mechanical Production Systems Engineering 2003: 61–5.
2. Özel T, Altan T. Process simulation using finite element method – prediction of cutting forces, tool stresses and temperatures in high-speed flat end milling. Int J Mach Tools Manuf 2000; 40: 713–38.
3. Zheng Yang K, Pramanik A, Basak AK, Dong Y, Prakash C, Shankar S, et al. Application of coolants during tool-based machining – A review. Ain Shams Engineering Journal 2023; 14: 101830. https://doi.org/10.1016/j.asej.2022.101830
4. Nguyen T-T, Mia M, Dang X-P, Le C-H, Packianather MS. Green machining for the dry milling process of stainless steel 304. Proc Inst Mech Eng B J Eng Manuf 2020; 234: 881–99. https://doi.org/10.1177/0954405419888126

5. Zhu L, Liu C. Recent progress of chatter prediction, detection and suppression in milling. Mech Syst Signal Process 2020; 143: 106840. https://doi.org/10.1016/j.ymssp.2020.106840
6. Kaliński KJ, Galewski MA. Chatter vibration surveillance by the optimal-linear spindle speed control. Mech Syst Signal Process 2011; 25: 383–99. https://doi.org/10.1016/j.ymssp.2010.09.005
7. [Kaliński KJ. A surveillance of dynamic processes in mechanical systems (in Polish). Gdansk: The Publication of Gdansk University of Technology; 2012.
8. Kalinski KJ, Galewski MA. Optimal spindle speed determination for vibration reduction during ball-end milling of flexible details. Int J Mach Tools Manuf 2015; 92: 19–30. https://doi.org/10.1016/j.ijmachtools.2015.02.008
9. Ercetin A, Aslantaş K, Özgün Ö, Perçin M, Chandrashekarappa MPG. Optimization of machining parameters to minimize cutting forces and surface roughness in micro-milling of Mg13Sn alloy. Micromachines (Basel) 2023; 14: 1590. https://doi.org/10.3390/MI14081590
10. Kaliński KJ, Mazur MR, Galewski MA. The optimal spindle speed map for reduction of chatter vibration during milling of bow thruster blade. Solid State Phenomena 2013; 198: 686–91. https://doi.org/10.4028/www.scientific.net/SSP.198.686
11. Vavruska P, Bartos F, Stejskal M, Pesice M, Zeman P, Heinrich P. Increasing tool life and machining performance by dynamic spindle speed control along toolpaths for milling complex shape parts. J Manuf Process 2023; 99: 283–97. https://doi.org/10.1016/J.JMAPRO.2023.04.058
12. Wang W, Guo Q, Yang Z, Jiang Y, Xu J. A state-of-the-art review on robotic milling of complex parts with high efficiency and precision. Robot Comput Integr Manuf 2023; 79: 102436. https://doi.org/10.1016/j.rcim.2022.102436
13. Li Z, Zeng Z, Yang Y, Ouyang Z, Ding P, Sun J, et al. Research progress in machining technology of aerospace thin-walled components. J Manuf Process 2024; 119: 463–82. https://doi.org/10.1016/j.jmapro.2024.03.111
14. Kurpiel S, Zagórski K, Cieślik J, Skrzypkowski K, Brostow W. Evaluation of the Vibration signal during milling vertical thin-walled structures from aerospace materials. Sensors 2023; 23: 6398. https://doi.org/10.3390/S23146398
15. Yan S, Sui L, Wang S, Sun Y. On-line tool wear monitoring under variable milling conditions based on a condition-adaptive hidden semi-Markov model (CAHSMM). Mech Syst Signal Process 2023; 200: 110644. https://doi.org/10.1016/j.ymssp.2023.110644
16. Bao Y, Wang B, He Z, Kang R, Guo J. Recent progress in flexible supporting technology for aerospace thin-walled parts: A review. Chinese Journal of Aeronautics 2022; 35: 10–26. https://doi.org/10.1016/j.cja.2021.01.026
17. Quintana G, Ciurana J. Chatter in machining processes: A review. Int J Mach Tools Manuf 2011; 51: 363–76. https://doi.org/10.1016/j.ijmachtools.2011.01.001
18. Wu G, Li G, Pan W, Raja I, Wang X, Ding S. A state-of-art review on chatter and geometric errors in thin-wall machining processes. J Manuf Process 2021; 68: 454–80. https://doi.org/10.1016/j.jmapro.2021.05.055
19. Budak E, Altintas Y. Analytical prediction of chatter stability in milling—part II: application of the general formulation to common milling systems. J Dyn Syst Meas Control 1998; 120: 31–6. https://doi.org/10.1115/1.2801318
20. Sun Y, Yan S, Sun S, Niu J, Xu J, Chen M, et al. A review of chatter suppression in thin-wall milling: strategies, mechanisms, and applications. International Journal of Extreme Manufacturing 2025; 7: 062003. https://doi.org/10.1088/2631-7990/adec24
21. Fei J, Lin B, Xiao J, Ding M, Yan S, Zhang X, et al. Investigation of moving fixture on deformation suppression during milling process of thin-walled structures. J Manuf Process 2018; 32: 403–11. https://doi.org/10.1016/j.jmapro.2018.03.011
22. Wang X, Zhao B, Ding W, Pu C, Wang X, Peng S, et al. A short review on machining deformation control of aero-engine thin-walled casings. The International Journal of Advanced Manufacturing Technology 2022; 121: 2971–85. https://doi.org/10.1007/s00170-022-09546-w
23. Gameros A, Lowth S, Axinte D, Nagy-Sochacki A, Craig O, Siller HR. State-of-the-art in fixture systems for the manufacture and assembly of rigid components: A review. Int J Mach Tools Manuf 2017; 123: 1–21. https://doi.org/10.1016/j.ijmachtools.2017.07.004
24. Liu H, Wang C, Li T, Bo Q, Liu K, Wang Y. Fixturing technology and system for thin-walled parts machining: a review. Frontiers of Mechanical Engineering 2022; 17: 55. https://doi.org/10.1007/s11465-022-0711-5
25. Zagórski K. Cutting forces during milling of vertical thin-walled structures of aerospace alloys. Advances in Science and Technology Research Journal 2025; 19: 197–210. https://doi.org/10.12913/22998624/203976
26. Altintas Y, Budak E. Analytical prediction of stability lobes in milling. CIRP Ann Manuf Technol 1995; 44: 357–62. https://doi.org/10.1016/S0007-8506(07)62342-7

27. Meshreki M, Attia H, Kövecses J. Development of a new model for the varying dynamics of flexible pocket-structures during machining. J Manuf Sci Eng 2011; 133: 041002–14. https://doi.org/10.1115/1.4004322
28. Munoa J, Iglesias A, Olarra A, Dombovari Z, Zatarain M, Stepan G. Design of self-tuneable mass damper for modular fixturing systems. CIRP Annals 2016; 65: 389–92. https://doi.org/10.1016/j.cirp.2016.04.112
29. Sarath S, Paul PS. Application of smart fluid to control vibration in metal cutting: a review. World Journal of Engineering 2021; 18: 458–79. https://doi.org/10.1108/WJE-06-2020-0232
30. Radu P, Schnakovszky C. A review of proposed models for cutting force prediction in milling parts with low rigidity. Machines 2024; 12: 140. https://doi.org/10.3390/machines12020140
31. Liu S, Xiao J, Zhao W, Zhao Y, Wang M, Liu H, et al. Dynamic characteristics and chatter prediction of thin-walled workpieces in dual-robot mirror milling based on surrogate model of support parameters. Mech Syst Signal Process 2025; 224: 112187. https://doi.org/10.1016/j.ymssp.2024.112187
32. Kaliński KJ, Galewski MA, Mazur MR, Morawska N. Minimization of vibrations during milling of flexible structures using mechatronic design techniques. Proceedings of the 2019 20th International Carpathian Control Conference, ICCC 2019, 2019. https://doi.org/10.1109/CarpathianCC.2019.8765681
33. Kaliński KJ, Galewski MA. A modified method of vibration surveillance by using the optimal control at energy performance index. Mech Syst Signal Process 2015; 58–59: 41–52. https://doi.org/10.1016/j.ymssp.2014.12.009
34. Kaliński KJ, Galewski MA, Mazur M, Chodnicki M. Modelling and simulation of a new variable stiffness holder for milling of flexible details. Polish Maritime Res 2017; 24: 115–24. https://doi.org/10.1515/pomr-2017-0029
35. Kaliński KJ, Galewski MA. Vibration surveillance supported by Hardware-In-the-Loop Simulation in milling flexible workpieces. Mechatronics. Elsevier Ltd. 2014; 24; 1071–82. https://doi.org/10.1016/j.mechatronics.2014.06.006
36. Kaliński KJ, Galewski MA, Mazur MR, Stawicka-Morawska N. Experimentally aided operational virtual prototyping to predict best clamping conditions for face milling of large-size structures. Applied Sciences 2024; 14: 7346. https://doi.org/10.3390/app14167346
37. Kruszewski J, Gawroński W, Wittbrodt E, Najbar F, Grabowski S. The rigid finite element method (in Polish). Warsaw: Arkady; 1975.
38. Fei J, Xu F, Lin B, Huang T. State of the art in milling process of the flexible workpiece. The International Journal of Advanced Manufacturing Technology 2020 109:5 2020; 109: 1695–725. https://doi.org/10.1007/S00170-020-05616-Z
39. Bąk R, Burczyński T. Strength of materials with elements of computer analysis (in Polish). Warsaw: The Scientific and Technical Publication; 2001.
40. Kaliński K. Vibration surveillance of mechanical systems which are idealized discretely (in Polish). Gdansk: The Publication of Gdansk University of Technology; 2001.
41. Gosiewski Z, Sawicki JT, Zabielski R. Vibration signals for rotating machine vibration for shaft cracking diagnostics (in Polish). Acta Mechanica et Automatica 2008; 2; 1; 27–33. https://pbc.biaman.pl/dlibra/doccontent?id=5175